



# High-Velocity Suspension Flame Sprayed (HVSFS) Hydroxyapatite Coatings for Biomedical Applications

N. Stiegler, D. Bellucci, G. Bolelli, V. Cannillo, R. Gadow, A. Killinger, L. Lusvarghi, and A. Sola

(Submitted June 29, 2011; in revised form November 23, 2011)

In this study, hydroxyapatite (HAp) coatings were deposited on Ti plates by the high-velocity suspension flame spraying (HVSFS) technique. The process characteristic, the microstructure and phase composition of the coatings are significantly influenced by the solvent and by the design of the combustion chamber (CC) of the HVSFS torch. Water-based suspensions always lead to fairly low surface temperatures ( $\approx 350$  °C), deposition efficiencies  $< 40\%$ , and produce coatings with low amount of crystalline HAp, which tend to dissolve very rapidly in simulated body fluid (SBF) solutions. DEG-based suspensions, when sprayed with properly-designed CCs, produce deposition efficiencies of 45-55% and high surface temperatures (550-600 °C). In these coatings, the degree of crystallinity increases from the bottom layer to the top layer, probably because the increasingly large surface temperature can eventually favour re-crystallisation of individual lamellae during cooling. These coatings are much more stable in SBF solutions.

**Keywords** biomedical applications, high-velocity suspension flame spraying (HVSFS), hydroxyapatite (HAp), simulated body fluid (SBF), thermal spraying

## 1. Introduction

The use of biocompatible coatings has become a common practice to enhance the osseointegration of endoprotheses such as hip and knee joint or dental implants. Remarkable increases in the number of hip and knee replacement surgeries are predicted. Primary total hip arthroplasty is estimated to grow by 174%, from 208,600 in 2005 to 572,100 by 2030, while primary total knee arthroplasty is projected to grow from 450,400 to 3.48 million procedures during the same period (more than 673% growth), just in the US (Ref 1).

The coatings generally consist of hydroxyapatite [ $\text{Ca}_5(\text{PO}_4)_3\text{OH}$ ] (HAp), which is chemically similar to the mineral component of human bone and hard tissue (Ref 2). It is indeed able to support bone in-growth and osseointegration when used in orthopaedic, dental, and maxillofacial applications (Ref 3, 4). Moreover, HAp

coatings have the capacity to shorten the healing process of metal based implants. These coatings are generally deposited by thermal spraying processes, because of their relatively low cost and ability to coat quite complex surfaces (Ref 5, 6). Specifically, atmospheric plasma-spraying (APS) and high velocity oxygen-fuel (HVOF)-spraying are well known deposition techniques for bioactive HAp coatings (Ref 7-13). The above mentioned processes are limited to conventional dry spray powder with a particle size greater than  $5 \mu\text{m}$ , because fluidization of the powder becomes more challenging with decreasing particle size. Dry feeding of micro-sized or nano-sized particles is only feasible by agglomerating them into granules larger than  $5 \mu\text{m}$ , as performed in Ref 13-15. While the use of nano-particle agglomerates may bring about some improvements in the mechanical properties (e.g. higher hardness and tensile adhesion strength), and, perhaps, in the biocompatibility of thermally-sprayed HAp, the coatings do not exhibit a real nanostructure. Thermally-sprayed lamellae obtained from nanostructured agglomerates indeed consist of a core-shell multi-modal microstructure, where the outer part has lost its original nanostructure due to melting and re-solidification, whereas the unmelted core retains some nanosized particles (Ref 13-15). Most importantly, these lamellae (Ref 15) have the same size as those obtained using conventional microstructured feedstock (Ref 16, 17), with diameters of some tens of micrometres and thicknesses of  $\geq 1 \mu\text{m}$ . Since homogeneous coatings can only be obtained by superimposing a very large number of lamellae, it is essential to reduce the average lamellar thickness in order to improve the quality of relatively thin ( $< 100 \mu\text{m}$ ) thermal spray layers, which is the case of most commercially-available HAp coatings (Ref 18-20). This goal, which is therefore of the utmost

N. Stiegler, R. Gadow, and A. Killinger, Institute for Manufacturing Technologies of Ceramic Components and Composites, University of Stuttgart, Allmandring 7b, 70569 Stuttgart, Germany; and D. Bellucci, G. Bolelli, V. Cannillo, L. Lusvarghi, and A. Sola, Department of Materials and Environmental Engineering, University of Modena and Reggio Emilia, Via Vignolesse 905, 41100 Modena, MO, Italy. Contact e-mail: nico.stiegler@ifkb.uni-stuttgart.de.

interest, can be attained by the direct spraying of individual micrometric particles or of micrometric agglomerates of nanoparticles. One way to accomplish this objective is to manufacture thermal spray coatings from suspension feedstock, instead of conventional dry powder. This indeed enables direct processing of micron-sized or nano-sized powder particles into the plasma or gas jet (Ref 21-26). Accordingly, compared to standard spray powder processing, direct processing of fine particles dispersed in liquid solvent always results in coatings with smaller lamella size (Ref 26, 27). One of the most promising suspension spray techniques is the high-velocity suspension flame spraying (HVSFS) process developed at Institute for Manufacturing Technologies of Ceramic Components and Composites (University of Stuttgart, Germany), proven to run as a stable process (Ref 28).

The present research therefore aims to ascertain how different process parameters like gas flow, air-fuel ratio and design of the combustion chamber (CC) of the HVSFS technique affect the coating properties and deposition efficiency.

## 2. Experimental

### 2.1 Suspension Composition

Two different HAp suspensions, supplied by Ce.Ri.Col. Centro Ricerche Colorobbia-Italy, were employed in the HVSFS experiments. Nano-sized HAp particles were dispersed either in diethylene glycol (DEG) or water. For

the water-based suspension, the solid content was 10 wt.% and for the diethylene glycol suspension it was 13 wt.%.

Samples of the raw material were investigated by scanning electronic microscopy (SEM), sputter-coated with gold and examined in a LEO VP 438 from Leo Elektronenmikroskopie GmbH, Oberkochen, Germany.

### 2.2 Deposition of the Coatings

The HVSFS spray torch was operated on six axis robot system following a meander shaped spray path with 2 mm meander offset. The substrates were planar 50 mm × 50 mm × 3 mm Ti (grade 2) plates, mounted vertically on a sample holder, degreased with acetone and mildly grit blasted using white corundum particles (FEPA 60; Ø = 210-300 µm) and 0.5 MPa compressed air, leading to a typical roughness of  $R_a = 2.5-4$  µm. The sample was cooled during the deposition by two air nozzles mounted on the torch. The samples were weighed before and after spraying, to determine the coating weight and calculate the deposition efficiency of different parameter sets. The surface temperature during coating process was monitored using a pyrometer type Keller Pz10 AF1. The coating parameters are summarized in Table 1.

As described in Ref 29, the feeding system of the HVSFS equipment continuously draws the suspension out of a reservoir and delivers it axially, under a controlled flow rate, into the CC of the HVSFS torch (modified HVOF torch, model: TopGun-G, GTV GmbH, Luckenbach, Germany). To feed the suspension into the CC, a conical shaped injection nozzle was used. For the spray experiments the torch was equipped with two differently designed CCs, referred to as “former CC design” and “advanced CC design” (Fig. 1). The former CC is conically shaped and has a smaller volume than the advanced CC. The advanced CC has a combined cylindrical-conical shape with an increased diameter.

### 2.3 Characterisation of Deposited Coatings

The as-deposited surface roughness was measured by a stylus profilometer (Perthometer PGK, Mahr, Göttingen, Germany). SEM (XL30, FEI, Eindhoven, the Netherlands) micrographs were taken from the surface and the polished cross-section (cold-mounted in polyester resin, ground with SiC papers and polished using diamond slurries up to 0.5 µm size and colloidal silica suspension) of each coating. Low magnification micrographs were

**Table 1** HVSFS deposition parameters

| Parameters                     | Settings                       |     |             |     |
|--------------------------------|--------------------------------|-----|-------------|-----|
|                                | #1                             | #2  | #3          | #4  |
| Suspension composition         | DEG based                      |     | Water-based |     |
| Fuel (propane) flow rate, slpm | 45 (propane)                   |     |             |     |
| O <sub>2</sub> flow rate, slpm | 265                            | 300 | 265         | 300 |
| Suspension flow rate, g/min    | 115                            |     | 105         |     |
| Stand-off distance, mm         | 125                            |     |             |     |
| Gun traverse speed, mm/s       | 600                            |     |             |     |
| Interpass spacing, mm          | 2                              |     |             |     |
| Number of cycles               | 10 (former CC)/3 (advanced CC) |     |             |     |

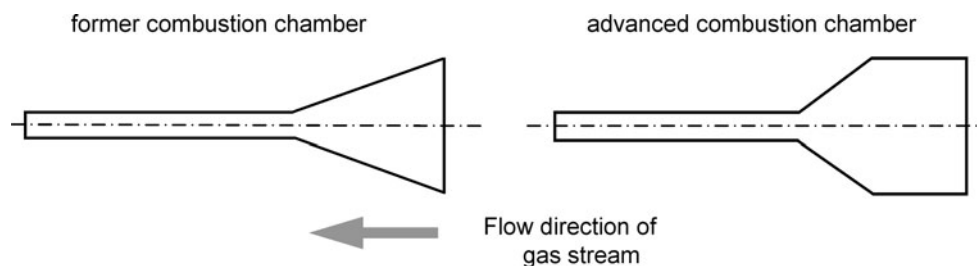


**Fig. 1** Schematic illustration of the two different CC designs of the HVSFS torch

employed in order to determine the coating thickness. The phase composition of the HAP coatings was analysed by x-ray diffraction (XRD: X'Pert PRO, PANalytical, Almelo, The Netherlands) on the surfaces of the coatings, both in as-deposited state and after grinding with 1200 mesh SiC papers. The pattern of the pure HAP powder was also taken as reference. Further structural investigations were carried out on as-deposited surfaces and polished cross-sections by micro-Raman spectrometry (Horiba Jobin-Yvon, Longjumeau, France: 632.81 nm-wavelength laser). As a reference, the spectra of the original HAP powder and of a TCP powder were also acquired.

The bond strength was measured according to ISO 4624 with a miniaturized measuring device on a universal testing machine Zwick Z100. HTK ULTRA BOND<sup>®</sup> was used as adhesive. Precipitation heat treatment of the glue took place at 190 °C for 35 min. The test speed was set to 0.5 mm/min.

To analyse the reactivity of the coatings, selected samples were immersed in a simulated body fluid (SBF) solution, prepared according to Kokubo and Takadama (Ref 30). The samples (10 mm × 10 mm squares, cut from the original plates) were immersed vertically in plastic containers filled with 20 mL of solution and were held at 37 °C in a controlled environmental chamber (MPM Instruments S.r.l., Bernareggio, MI, Italy). Soaking times were 1, 3, 7 and 14 days. The surfaces and polished cross-sections of the soaked samples were studied by SEM, XRD and micro-Raman spectroscopy.

### 3. Results and Discussion

#### 3.1 Suspension and Process Characterisation

The suspension properties are a significant aspect for the HVSFS coating process. During axial injection of the liquid feedstock into the CC of the HVSFS torch, the suspension jet gets atomized into small droplets by an injection nozzle (Ref 31-34). The liquid phase then evaporates rapidly from the droplets, releasing individual particles or (more frequently) particle agglomerates. Their size strongly influences their thermal history: small particles or small agglomerates rapidly heat up, but they also rapidly cool down resulting in a fairly different behaviour concerning the splat formation on the surface (Ref 34).

The evaporation of the liquid phase also causes cooling of the flame due to the enthalpy of vaporization. If the liquid phase is not water but a solvent like DEG, however, this effect is compensated by its additional combustion in the CC of the HVSFS torch, which leads to an increase of the thermal energy in the HVSFS system due to the enthalpy of combustion.

The highest surface temperature during the coating process was accordingly recorded using the DEG-based suspension (Fig. 2). A strong influence of the design of the CC on the maximum surface temperatures during the coating process could also be observed for the DEG-based suspension: specifically, the advanced CC design leads to a significant increase of the coating temperature using the

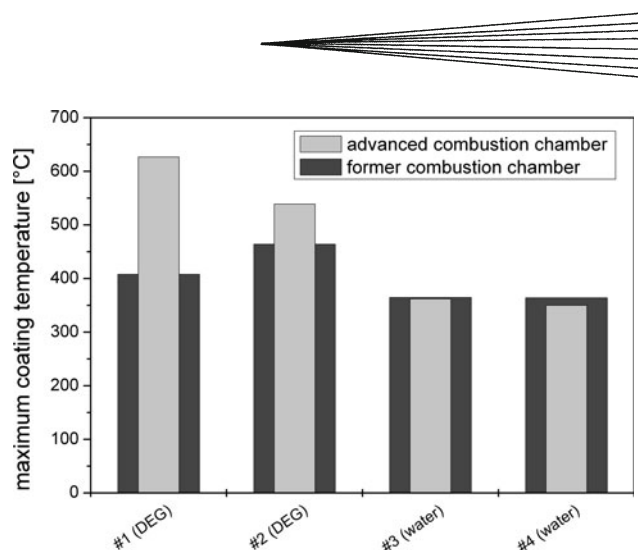


**Fig. 2** Recorded maximum surface temperature during HVSFS coating process for former and advanced CC design, each for parameter set #1-#4

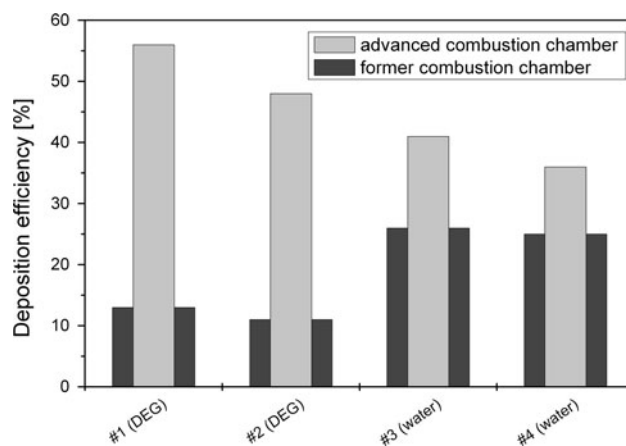


**Fig. 3** Measured deposition efficiency of the HVSFS deposited coatings for former and advanced CC design, each for parameter set #1-#4

DEG-based suspension (Fig. 2). For the parameter set #1, 408 °C were measured using the former CC design and 627 °C using the advanced CC design. For parameter set #2, the maximum surface temperature could be increased from 464 to 539 °C by changing the CC design. Using the water-based suspension no significant difference could be detected either for the two different CC designs, or for the different spray parameters. The measured maximum surface temperatures during the coating process using the water-based suspension were always around 360 °C.

Not only the maximum coating temperature is influenced by the design of the CC, but also the deposition efficiency could be drastically increased, see Fig. 3. The advanced CC design leads to higher deposition efficiency (a growth of 300% is obtained for DEG based suspension and of 75% for water based suspension) compared to the former design. Deposition efficiency of around 12% for the DEG-based suspension and 25% for the water-based

suspension could be reached with the former CC design. By modifying only the design of the CC to the so called “advanced CC design” and keeping all other parameters constant, the deposition efficiency could be increased up to 56% for the DEG-based and 41% for the water-based suspension. For the standard HVOF process the deposition efficiency also strongly depends on the process parameters and varies between 40 and 80% (Ref 35).

The coating deposition phenomena are also strongly influenced by the rheological behaviour of the suspension and by the particle agglomeration behaviour. The diethylene glycol suspension shows an almost Newtonian behaviour, whereas the water-based one exhibits a shear-thinning behaviour: the viscosity decreases with increasing shear rate (Fig. 4). Although pure water is a Newtonian fluid, its rheological behaviour changes remarkably with addition of solid particles.

Another important point is the stability of the suspension. Indeed, the used suspensions did not show any sedimentation, even after months of observation.

From SEM micrographs it can be stated that dispersed particles of the two suspensions consist of nano-sized (<50 nm) primary particles (Fig. 5).

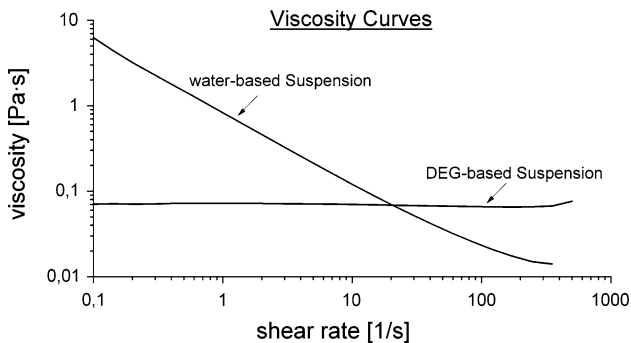


**Fig. 4** Viscosity curves of the water-based and DEG-based HAp suspensions

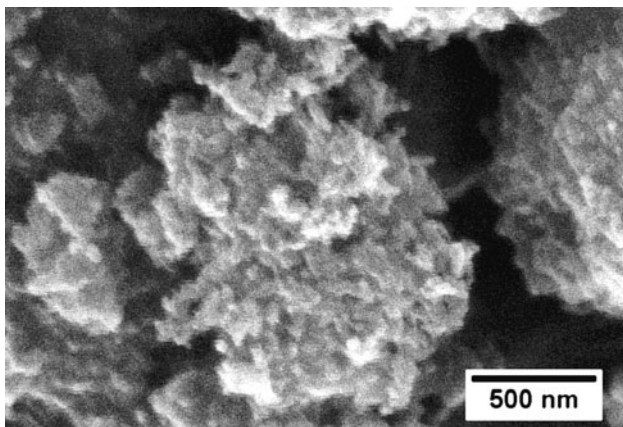


**Fig. 5** SEM micrograph (secondary electrons) of the HAp nanoparticles

### 3.2 Microstructural Properties of the Deposited Coatings

Remarkable differences exist between the various coatings, regarding both thickness and deposition efficiency.

Figure 6 summarizes the different microstructures of the HVSFS coatings sprayed with DEG- and water-based suspension by means of SEM micrographs. Regarding the HVSFS process, the use of diethylene glycol (Fig. 6a and b) or water (Fig. 6c and d) as solvent for the suspension affects the coating microstructure as much as the design of the used CC does affect the maximum coating temperature and deposition efficiency. For the experiments with the former CC design (Fig. 6a and c) 10 torch cycles were performed and for the experiments using the advanced CC design (Fig. 6b and d) the number of cycles was reduced to three, because of the higher deposition efficiency.

Conventional HVOF sprayed HAp coatings consist of unmelted submicron size particles and well flattened lamellae, depending on the process parameters like fuel-, oxygen flow rate and stand off distance (Ref 35).

The HVSFS coatings produced by the water-based suspension have a layered morphology, i.e. the layers deposited during each of the torch cycles performed during the deposition of this coating are clearly separated by porosity lines: this is particularly true for the coating deposited using the former CC design (Fig. 6c). The interlayer porosity contains numerous sub-micrometric rounded particles and agglomerates of partially unmelted nanoparticles (Fig. 7a, labels 1 and 2 respectively). Most probably, they were originated by re-solidified molten agglomerates and by unmelted agglomerates, respectively. Their larger abundance is consistent with the reduction in flame enthalpy brought about by water vaporisation, as put forward in Section 3.1, and also with the lower deposition efficiency produced by the former CC design. It may be speculated that this design produces slower, shorter flames which favour in-flight re-solidification of molten agglomerates, and/or that it results in fluid-dynamic effects which cause more agglomerates to reside in the colder fringes of the gas jet.

The diethylene glycol-based suspension produces denser coatings, where the individual layers are not so clearly recognizable (Fig. 6a). These coatings, however, are transversally micro cracked and definitely rougher than those obtained by the water-based suspension (Fig. 8): more specifically, some cone-shaped features propagate along the cross-section of these coatings (Fig. 6b and detailed view in Fig. 7b), starting from some defect site and ending up in surface “bumps” on top of which abundant fine particles are recognizable (Fig. 7b and 8a).

Two phenomena can concur to the formation of cone-shaped features. On the one hand, in accordance with Ref 20, the cone-shaped features can be ascribed to the propagation of originally small defects during layer-by-layer deposition. Micrometric imperfections of the underlying surface (caused e.g. by micrometric re-solidified agglomerates, etc.), which would not affect much the formation of large conventionally-sprayed droplets, can

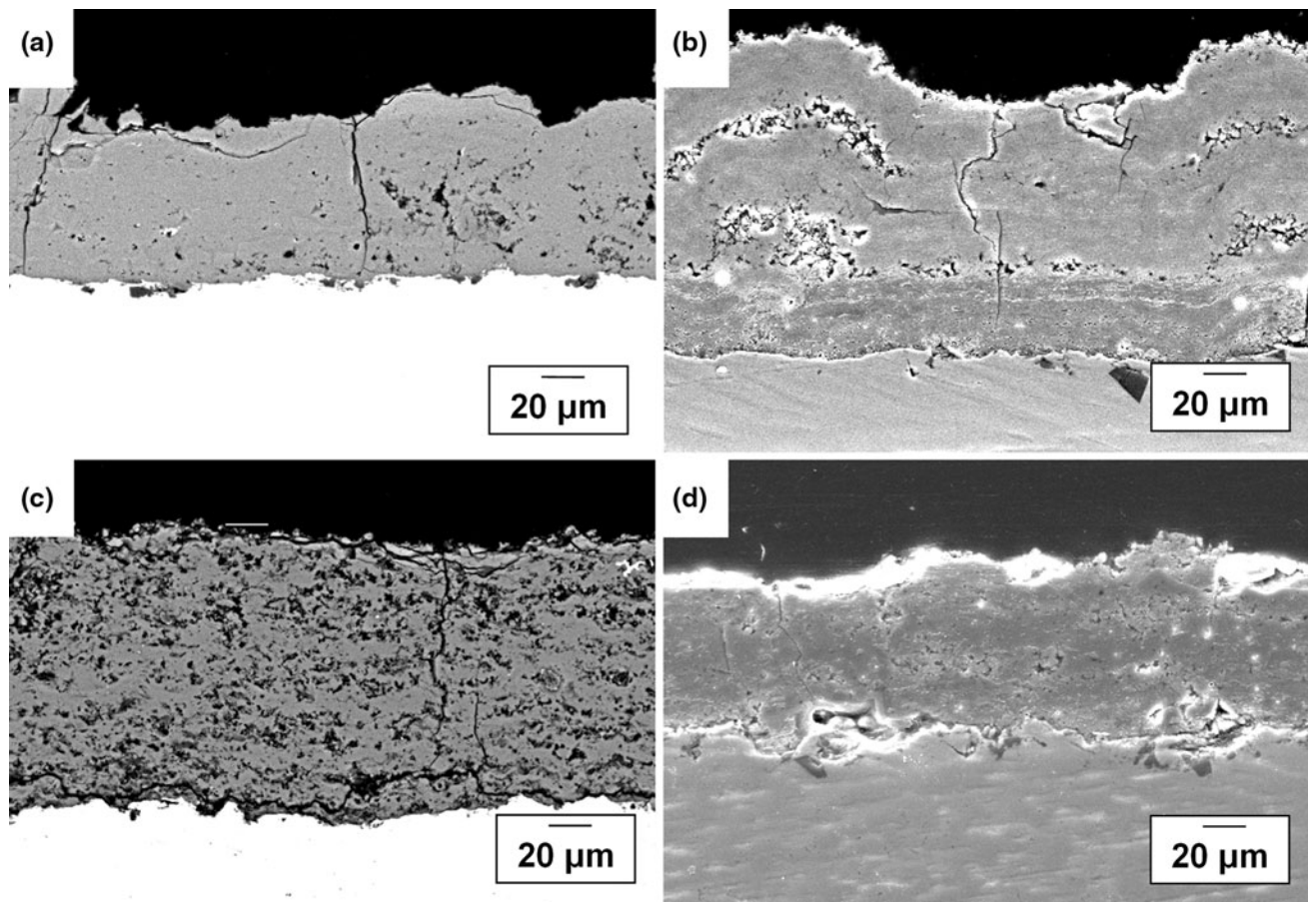


**Fig. 6** SEM micrographs of cross-sectional views: (a) DEG-based HAP coating, former CC design; (b) DEG-based HAP coating, advanced CC design; (c) water-based HAP coating, former CC design; and (d) water-based HAP coating, advanced CC design

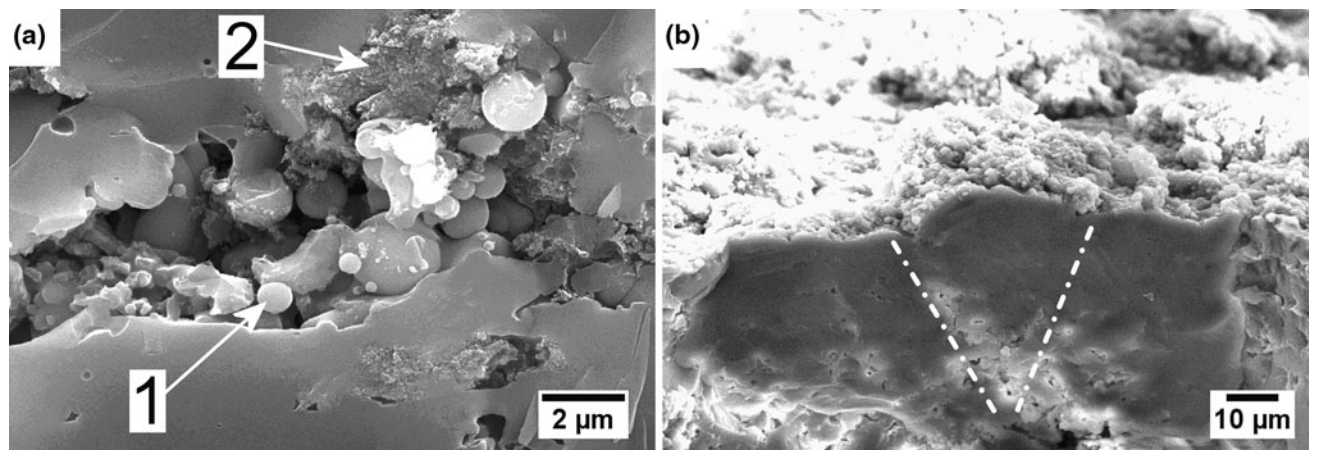


**Fig. 7** SEM micrographs of the fractured section of the water-based HAP coating, former CC design (a: label 1 = rounded sub-micron particle; label 2 = unmelted nanoparticles) and of the DEG-based HAP coating, former CC design (b: the dash-dot lines mark a cone-shaped defect)

perturb significantly the flattening of micrometric suspension-sprayed lamellae, whose size is comparable to that of the imperfection itself (Fig. 9). These lamellae can therefore be disrupted and generate new imperfections,

extending over a larger surface area (Ref 20). The defect therefore enlarges at every torch pass, developing into the cone-shaped feature. In the coatings deposited using water-based suspensions, the continuous growth of the

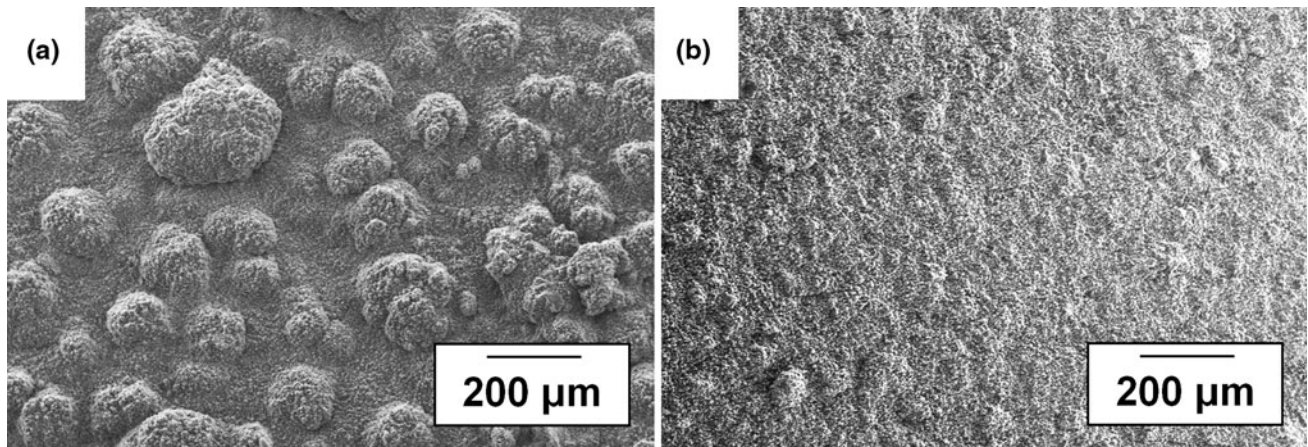


**Fig. 8** SEM micrographs of as-sprayed surfaces: (a) DEG-based HVFSFS HAp coating, new CC design and (b) water-based HVFSFS HAp coating, new CC design

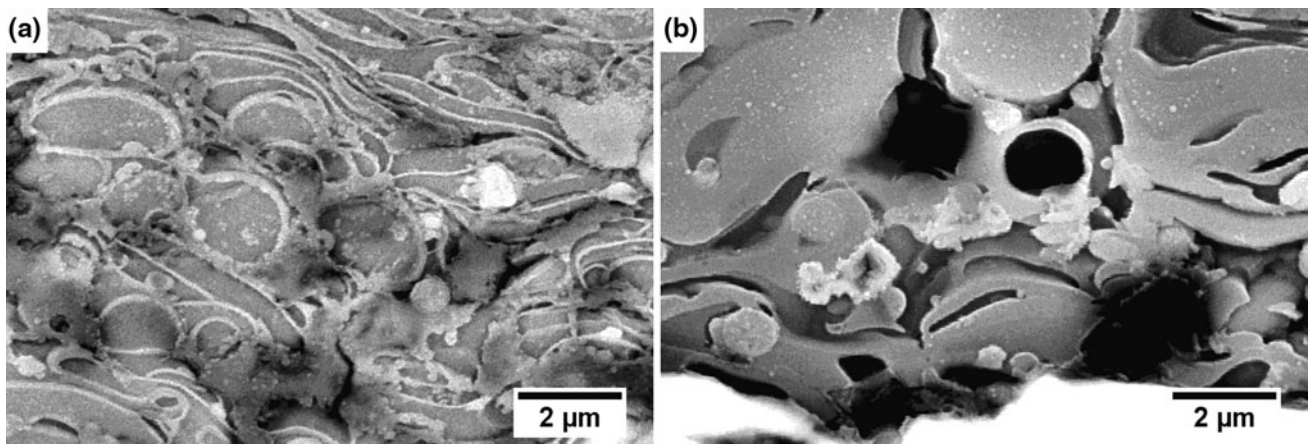


**Fig. 9** SEM details of the cross-sections of the water-based (a) and DEG-based (b) HVFSFS HAp coatings deposited using the new CC design

defect through the layers is interrupted by the large inter-layer porosity, so that the formation of cone-shaped features is hindered.

On the other hand, the particles and agglomerates in the HVFSFS gas jet, because of their very small size, might be deflected by the stagnation flow in front of the substrate. The mechanisms would be similar to those described in great detail in Ref 36 for the suspension plasma spraying process. The deflected particles, acquiring a velocity component parallel to the substrate surface, would have greater probability to attach to some prominent asperity than to the surrounding flat surface: the coating would therefore grow faster on asperities than on the surrounding surface, leading to the formation of a cone-shaped feature. Additional comments on the possibility of particle deflection during HVFSFS, based on fundamental fluid-dynamics considerations, are presented in Section 3.4.

The diameters of the fine lamellae existing inside each layer (Fig. 9) are generally comprised between 2 and 6  $\mu\text{m}$

(average value  $\approx 4 \mu\text{m}$ ) and their thickness varies between 200 and 500 nm (average value  $\approx 300 \text{ nm}$ ), consistently with the expectations put forward in the Introduction and regardless of the use of DEG- or water-based suspensions. The lamellae were presumably produced by molten droplets of  $\approx 0.5\text{--}2 \mu\text{m}$  radius, if it is assumed that lamellae and original molten droplets have equivalent volumes. The average flattening ratio is therefore  $\approx 2$ . All of these values match quite well with the corresponding ones observed in a previous study on HVFSFS  $\text{Al}_2\text{O}_3$  coatings (Ref 37). In order to give rise to a flattened lamella, agglomerates of HAp nanoparticles with radii of  $0.5\text{--}2 \mu\text{m}$  (“sprayability window”) should therefore be developed in the suspension, as previously identified for  $\text{Al}_2\text{O}_3$  particles and agglomerates too (Ref 37), quite independently of the specific solvent (water or DEG). Finer agglomerates are melted, but they re-solidify before impact, giving rise to rounded inclusions of  $\leq 1 \mu\text{m}$  diameter, which are indeed seen in the present layers (Fig. 9) together with the flattened lamellae. Similar rounded inclusions were accordingly

found in HVSFS  $\text{Al}_2\text{O}_3$  coatings obtained from nanoparticle suspensions (Ref 37). Larger agglomerates are unmelted, and they can give rise to interlayer defects.

The differences between the observed deposition efficiency values (Fig. 3) can therefore be ascribed both to the different behaviour of the solvent (as mentioned in Section 3.1) and to the different droplet fragmentation processes, which affect the final size distribution of the agglomerates within the spray jet. Modelling work will probably be needed in order to get a complete understanding of these processes, since complex phenomena are occurring: for instance, previous work has shown that the suspension injection geometry and the process conditions may even shift solvent vaporisation from the CC to the expansion nozzle (Ref 38). More specifically, in the present case it can be speculated that an additional reason why the deposition efficiency of the water-based suspension never increases too much, apart from the obvious cooling effect of water on the combustion flame (mentioned in Section 3.1 and reflected by the lower maximum substrate temperature values in Fig. 2), lies in the rheological properties of that suspension: its plastic behaviour (Fig. 4) indeed suggests a tendency to flocculate, developing large agglomerates, which presumably cannot be entirely disrupted after injection in the CC.

### 3.3 Coating Structure

X-ray diffraction patterns acquired on the as-deposited coatings lead to the conclusion that the coatings produced by HVSFS using DEG-based suspensions are richer in crystalline HAp than those obtained using water-based suspensions (Fig. 10). The highest amount of crystalline HAp was achieved for the coatings sprayed using the advanced CC design with the DEG-based suspension. Minor amounts of TTCP and  $\beta$ -TCP are also found: they could be produced by crystallisation during the in-flight re-solidification of small agglomerates (the in-flight re-solidification process is indeed much slower than the impact quenching of molten droplets) or by thermal alteration of HAp in some of the unmelted agglomerates. All patterns were acquired under the same experimental conditions.

In Fig. 11, details of the different microstructures are presented by means of SEM images and micro-Raman spectroscopy. The coatings produced with the advanced CC design using the water-based suspension show a uniform microstructure and amorphous calcium phosphate is the most abundant phase in all three layers of the coatings (Fig. 11b). Using the DEG-based suspension and the same process parameters the bottom layer deposited during the first torch cycle has a fairly different microstructure compared to the layers of the second and third torch cycle. For the DEG-based coatings the most abundant phase of the bottom layer is amorphous calcium phosphate (Fig. 11a), whereas the middle and top layer show a high amount of crystalline HAp, together with minor peaks, presumably belonging to TTCP and  $\beta$ -TCP (Ref 39, 40), consistently with XRD patterns (Fig. 10).

In conventionally-sprayed HAp coatings, high degrees of crystallinity can only be obtained by retaining

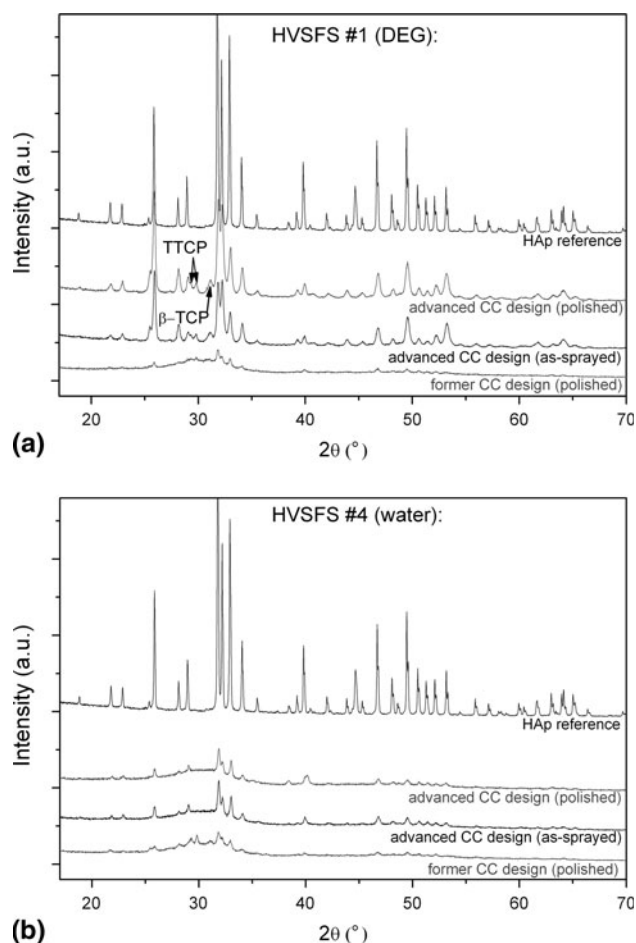


**Fig. 10** XRD patterns of the polished and unpolished HAp coatings. The pattern of a pure HAp powder is provided for reference: coatings sprayed with (a) DEG-based suspension and (b) water-based suspension; results for both, former and advanced CC design are displayed

significant amounts of unmelted material (Ref 41, 42), whereas molten particles mostly develop amorphous calcium phosphate, since their cooling rate, especially upon impact-quenching, is too large to allow completion of the slow and complex crystallization process of HAp, which is particularly difficult because of the incongruent melting of this (Ref 43). In all of the present HVSFS coatings, the dense layers were mainly originated by molten agglomerates, which solidified either onto the substrate (producing flattened lamellae) or in-flight (producing rounded particles). The mainly amorphous structure of the HVSFS coatings deposited using the water-based suspension (regardless of the CC design) and of those obtained using the DEG-based suspension and the former CC design, revealed by XRD patterns and by micro-Raman spectra, is therefore in excellent accordance with the mechanisms outlined in Ref 41 and 42. Most of the small fraction of crystalline HAp in those coatings is probably contributed by the few unmelted agglomerates contained in the inter-layer regions described in Section 3.2. Some of the re-solidified droplets contained both in the inter-layer area

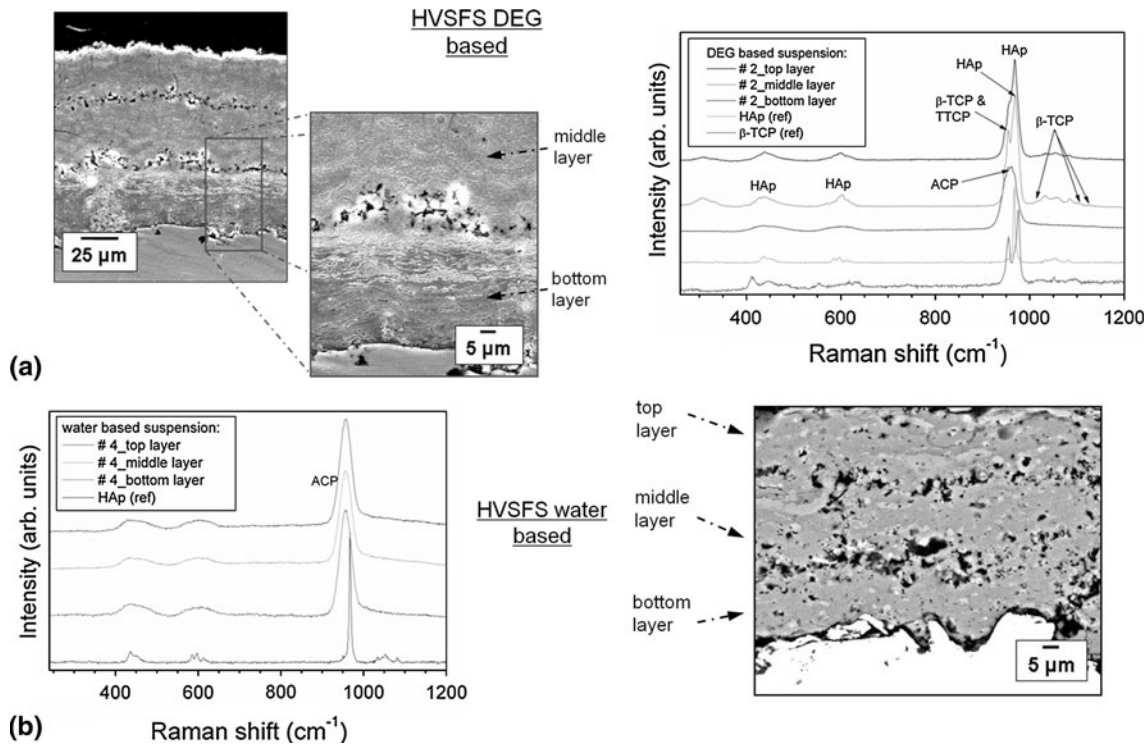


**Fig. 11** SEM micrographs of cross-sectional views and analogous micro Raman spectra: coatings sprayed with advanced CC (a) DEG-based HVSFS HAp coating and (b) water-based HVSFS HAp coating

and inside the layer may also include some crystalline phases, as in-flight cooling is somewhat slower than impact quenching, as mentioned previously.

By contrast, the behaviour of the coatings obtained by spraying the DEG-based suspension using the advanced CC design, which are associated to the highest system temperatures (Fig. 2), is completely different: they indeed attained high degrees of crystallinity. Specifically, the layer deposited during the first torch cycle, when the average temperature of the substrate surface (monitored by the pyrometer, Section 2.2) was still around 300 °C, is mainly amorphous, while crystalline layers (containing large amounts of HAp with minor amounts of TTCP and  $\beta$ -TCP) were produced during the second and third cycles (Fig. 11), as the system temperature increased to values > 500 °C, as shown in Fig. 2.

The most obvious explanation for this phenomenon is the in situ re-crystallisation of the sprayed lamellae, induced by the large average temperature of the deposited layer. The cooling rate of a lamella is large ( $\geq 10^7$  K/s, Ref 44) immediately after its impact, when its temperature is significantly higher than that of the surrounding material, but, as this difference is reduced, the cooling rate decreases. Since the average temperature of the third layer is 500-600 °C (Fig. 2), each lamella can remain at temperatures close to 1000 °C for a significant period (some tens of seconds) and undergo significant re-crystallisation.

This hypothesis can be corroborated by considerations based on the re-crystallization kinetics of amorphous calcium phosphate in thermally-sprayed HAp coatings.

Chang et al. (Ref 45) indeed showed that the conversion degree  $\alpha$  of the amorphous phase ( $\alpha=0$ : no conversion;  $\alpha=1$ : complete re-crystallisation) during high-temperature annealing of those coatings is described by Eq 1:

$$\frac{1}{1-\alpha} = kt + C \quad (\text{Eq 1})$$

where  $t$  is the time;  $C$  the integration constant ( $C=0$  if the initial conversion degree is zero); and  $k$  is the proportionality coefficient with Arrhenius-type temperature dependence ( $T$ =temperature):

$$k = e^{-(E_a/RT)}$$

Assuming  $C=0$ , the following relation (2) therefore links the conversion degrees attained after the same time period  $t$  at two different temperatures  $T_1$  and  $T_2$ :

$$\ln\left(\frac{1-\alpha_2}{1-\alpha_1}\right) = -\frac{E_a}{R}\left(\frac{1}{T_1} - \frac{1}{T_2}\right) \quad (\text{Eq 2})$$

The parameter  $(1-\alpha)$  indicates the fraction of unconverted (non-crystallised) amorphous calcium phosphate. By using the value of the activation energy  $E_a = 11.31 \cdot 10^4$  J/mol computed in Ref 45, the relation between the conversion degrees at  $T_1 = 600$  °C (873 K) and at  $T_2 = 1000$  °C (1273 K) is:

$$\ln\left(\frac{1-\alpha_2}{1-\alpha_1}\right) = -4.9 \rightarrow \frac{1-\alpha_2}{1-\alpha_1} \approx 7.4 \times 10^{-3} \quad (\text{Eq 3})$$

This means that, while at 600 °C many hours of treatment are needed in order to obtain significant conversion



degrees (Ref 45), the conversion at about 1000 °C is extremely fast, and can lead to significant amounts of crystalline phase in the few tens of seconds which are allowed to a lamella before it reaches the average system temperature.

This process could not take place while spraying the water-based suspension or while spraying the DEG-based one with the former CC design: in that case, indeed, the average system temperature was too low and caused the cooling rate of the lamellae to be still very high at 1000 °C. Analogously, while spraying the first coating layer using the DEG-based suspension and the advanced CC design, the average system temperature was still not large enough.

This result also indicates that crystalline phases are not formed after the lamella has attained the average system temperature and that an amorphous layer cannot be re-crystallised after its deposition (during the spraying of subsequent layers): at 500-600 °C, re-crystallisation of previously-deposited material would indeed require hours (as mentioned above) and is consequently not possible in the relatively brief duration (no more than 10 min overall) of the whole HVFSFS deposition process.

### 3.4 Surface Roughness

In Fig. 8 the different surface topography of the HVFSFS coatings sprayed with DEG- and water-based suspension by means of SEM images are summarized. Fine re-solidified spherical droplets and unmelted agglomerates seem to concentrate around asperities of the coating surface.

The deposition mechanism of the single particles is depending on the inertia of the particles. The Stokes number is an important scaling parameter in fluid-particle flows, which describes the ratio of particle response time  $\tau_R$  to a time characteristic of the fluid motion  $\tau_F$ . A Stokes number  $St \ll 1$  denotes that the spray particles can maintain near velocity equilibrium with the gas fluid while a large Stokes number  $St \gg 1$  suggests that the spray particle motion is unaffected by the gas flow field in the CC and also near the substrate surface (Ref 46).

According to Ref 47,  $\tau_R = \rho_P d_P^2 / (18 \mu_g)$  (where  $\rho_P$ ,  $d_P$  is the density and diameter of the droplet and  $\mu_g$  is the dynamic viscosity of the gas flow) is the particle response time to viscous drag by the gas flow and  $\tau_F = d/U$  (where  $d$  is the characteristic length associated to the gas flow and  $U$  is the gas flow velocity) is the characteristic time of fluid motion in the HVOF gas jet. For small ( $d_P \leq 1 \mu\text{m}$ ) HAP droplets ( $\rho_P \approx 3.2 \text{ g/cm}^3$ ), assuming  $\mu_g \approx 7 \times 10^{-5} \text{ Pa s}$  (Ref 48),  $d \approx 8 \text{ mm}$ ,  $U \approx 1500 \text{ m/s}$  (Ref 38), the Stokes number is  $St = \tau_R / \tau_F \leq 0.5$ , whereas, in a conventional HVOF process with  $d_P \approx 20 \mu\text{m}$ ,  $St = \tau_R / \tau_F \approx 190$ .

Differently from a conventional HVOF process, where particles are quite insensitive to gas flow perturbations (e.g. turbulent eddies) and can easily travel beyond the stagnation flow in front of the substrate, the finest HVFSFS droplets tend to copy the gas flow characteristics because of their low inertia. They can therefore be ejected from the flow axis by the effect of shock diamonds, be caught in the cold jet fringes and be deflected by the turbulent flow

in front of the substrate. This is confirmed by numerical simulations in Ref 49. Deflected particles travel horizontally along the coating surface and stick preferentially to some prominent asperities. In addition to this, a non-uniform surface characteristic is well developed in the DEG-sprayed samples (Fig. 8a) as a consequence of the cone-shaped defects described in Section 3.2. These cone-shaped features indeed result in a surface “bump”, as previously reported in Ref 50, and this is most likely to cause the high surface roughness values which were experimentally measured. In fact the DEG-based suspension leads to a surface roughness of  $R_a = 12.5 \mu\text{m}$  and  $R_z = 68 \mu\text{m}$ . The surface roughness of the water-based coatings depends on the design of the CC. The former CC design leads to surface roughness of  $R_a = 9.3 \mu\text{m}$  and  $R_z = 56 \mu\text{m}$ , the advanced CC design to  $R_a = 4.8 \mu\text{m}$  and  $R_z = 35 \mu\text{m}$ .

### 3.5 Adhesion Strength of As-Deposited Coatings

The bond strength values, measured using the pull-off method, are displayed in Fig. 12. The bond strength of the deposited HAP coatings is dependent on the spray process and the spray parameters. In literature bond strength values between 5 and 23 MPa for APS (Ref 51) and  $24 \pm 8 \text{ MPa}$  for HVOF (Ref 14) HAP coatings can be found. Since the preparation of the substrate surface has a significant influence on the adhesion strength of the coating, all used substrates were treated under the same conditions. All of the HVFSFS coatings, regardless of the deposition method, exhibit analogous average tensile adhesion strength values, close to 20 MPa and similar to that of the APS-HAP coatings (Fig. 12).

### 3.6 Simulated Body Fluid (SBF) Test

The behaviour of the HVFSFS-deposited HAP coatings during immersion in the SBF solution depends on their crystallinity. Coatings with poor crystallinity dissolve rapidly, because of the high reactivity of amorphous calcium phosphate, and saturate the solution with Ca and P,

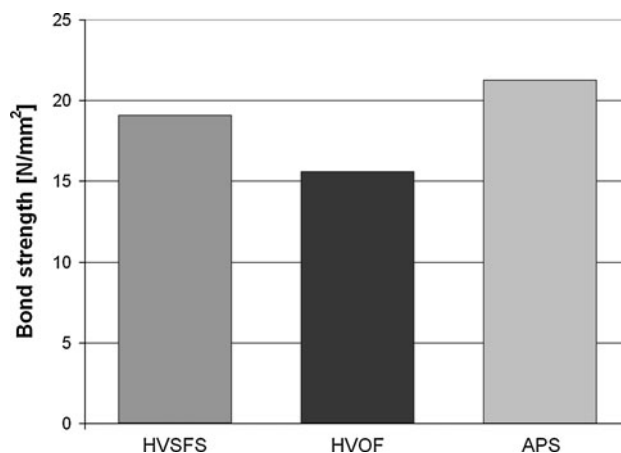


Fig. 12 Measured bond strength for the HVFSFS, HVOF and APS deposited HAP coatings

causing the re-precipitation of a HAp layer on their own surface (Fig. 13a). This precipitated film is definitely similar to that described in previous studies on conventional thermally-sprayed HAp (Ref 52, 53).

More specifically, cross-sectional views reveal that, after 1 day, the lamellae exhibit an “etched” morphology, probably because those containing the largest amounts of amorphous phase had already started to dissolve (Fig. 13b). After 3 days, HAp precipitated as a film on top of the coating (Fig. 13c, label 1) as well as in some pores and defects inside the coating (Fig. 13c, label 2). After soaking for 14 days, almost 1/3 of the coating thickness has been dissolved and replaced by the precipitated layer (Fig. 13d). The continuous growth of this HAp layer is witnessed by the evolution of the XRD patterns (Fig. 14a), where the amorphous band is progressively replaced by broad peaks of increasingly large intensity, all belonging to crystalline HAp, and of the micro-Raman spectra (Fig. 14b), where, even after 1 day, the broad

peaks of the amorphous phase are substituted by the sharp peaks of crystalline HAp. Some of the micron-sized rounded particles existing in the coatings (Section 3.2) can be recognised inside the precipitated layer (Fig. 13c and d: label 3). This observation confirms the previous hypothesis on the presence of some crystalline phases inside those droplets, as a consequence of the slower in-flight re-solidification process (Section 3.3): their presence indeed reduces their solubility in the SBF solution.

These observations indicate that amorphous HVSFS HAp coatings have very low stability in body fluids; the presence of rounded particles in the precipitated layer also implies the possible risk of a release of micrometric particles inside the tissues, which might elicit inflammatory responses (Ref 54).

Much better stability is exhibited by the highly crystalline coatings obtained by spraying the DEG-based suspension using the advanced CC design: in this case, minimal dissolution occurred (no thickness reduction and

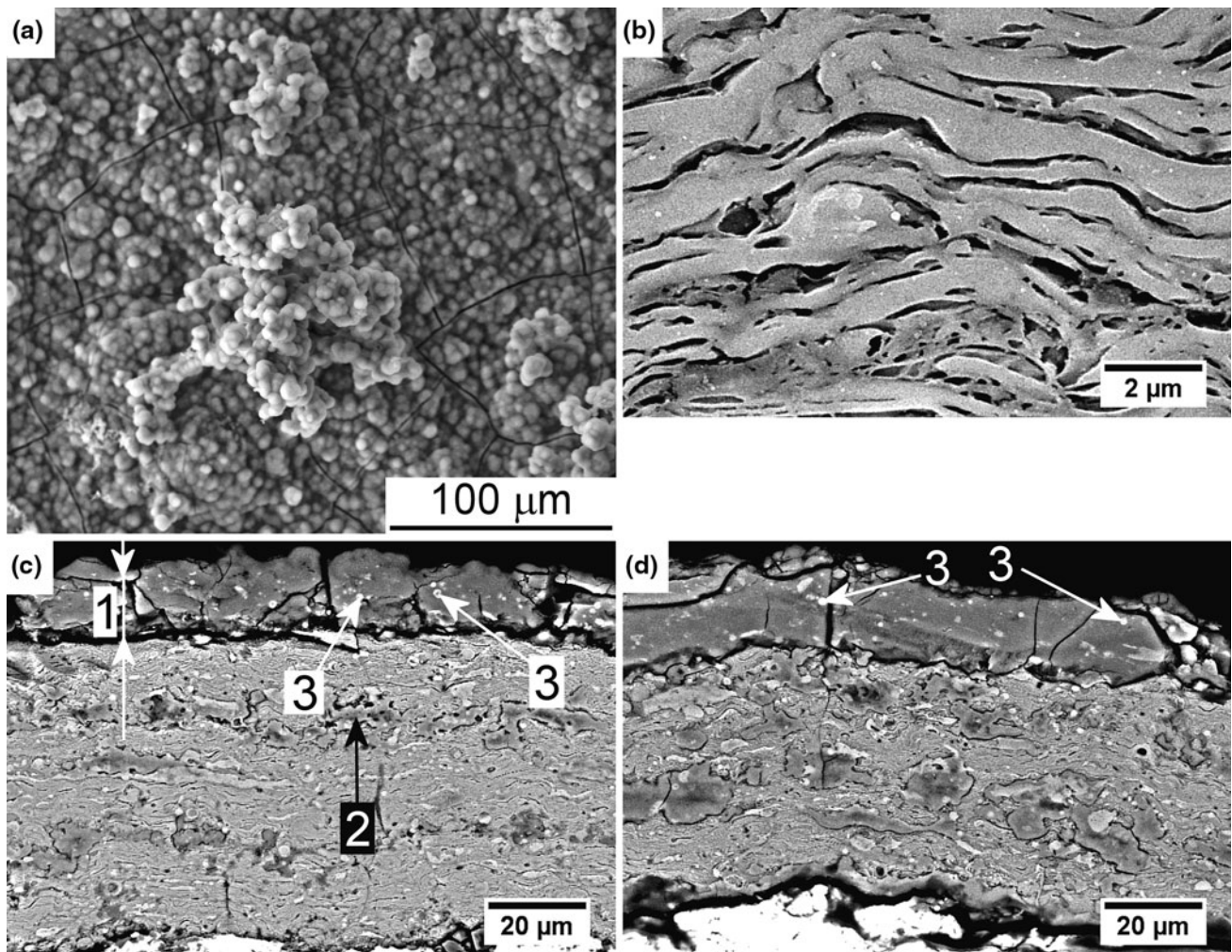


**Fig. 13** Top surface of the water-based HVSFS HAp coating (advanced CC design) after soaking in SBF for 7 days (a), cross-sectional detail of “etched” lamellae after soaking for 1 day (b), and cross-sectional overviews after soaking for 3 days (c) and 14 days (d). Label 1 = HAp precipitated onto the coating; label 2 = HAp precipitated inside inter-layer defects; label 3 = micrometric rounded particles included in the precipitated film

no precipitation of a continuous film, even after 2 weeks of soaking in SBF: Fig. 15a), which is also witnessed by the lack of significant changes in the XRD patterns (Fig. 14c). Raman peaks become slightly sharper after soaking (Fig. 14d), probably because of the dissolution of minor amounts of amorphous phase from the topmost layer.

The different behaviours of the HVSFs HAp coatings as a function of their crystallinity resembles the differences previously noted between highly crystalline VPS HAp coatings and mainly amorphous detonation gun-

sprayed coatings (Ref 52). This indicates, on the one hand, that the HVSFs process is highly flexible and can produce coatings with different reactivity (stable crystalline coatings or fast-reacting amorphous layers) and, on the other hand, that the HVSFs processing does not modify the typical reactivity of HAp-based materials.

Limitations, however, still exist. In the bottom layer of the coating obtained by spraying the DEG-based suspension using the advanced CC design, indeed, “etching” of the lamellae can be recognised (Fig. 15b), similarly to the

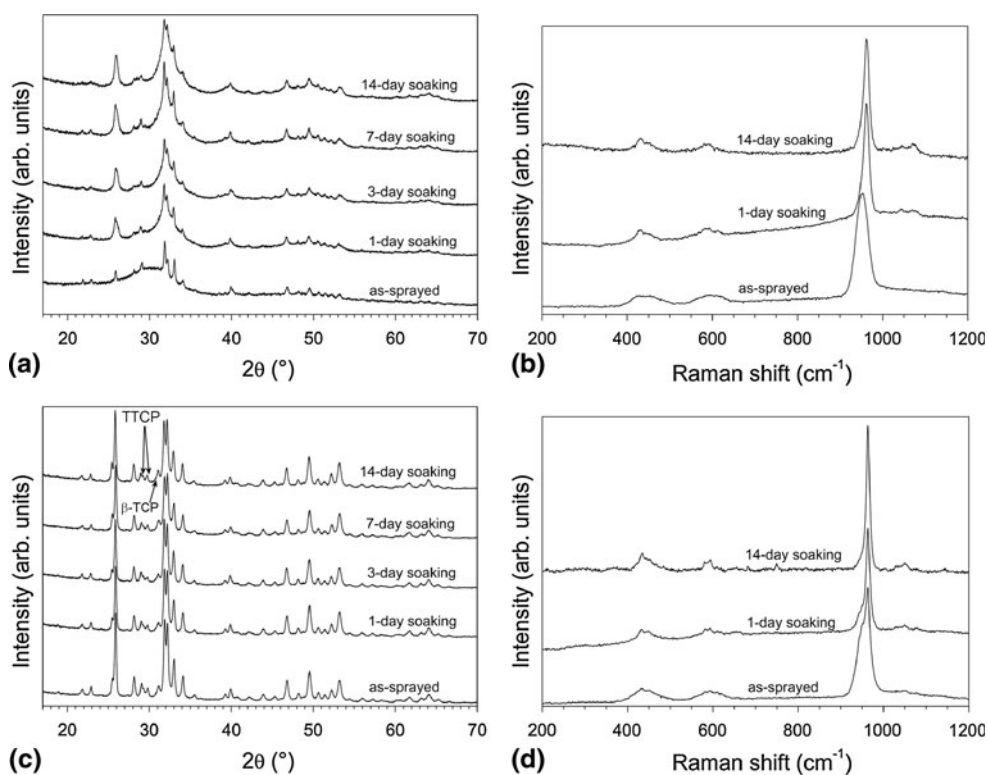


**Fig. 14** Evolution of the XRD patterns (a, c) and of the Raman spectra (b, d) of the water-based (a, b) and DEG-based (c, d) HAp coatings (advanced CC design) after soaking in SBF for various times

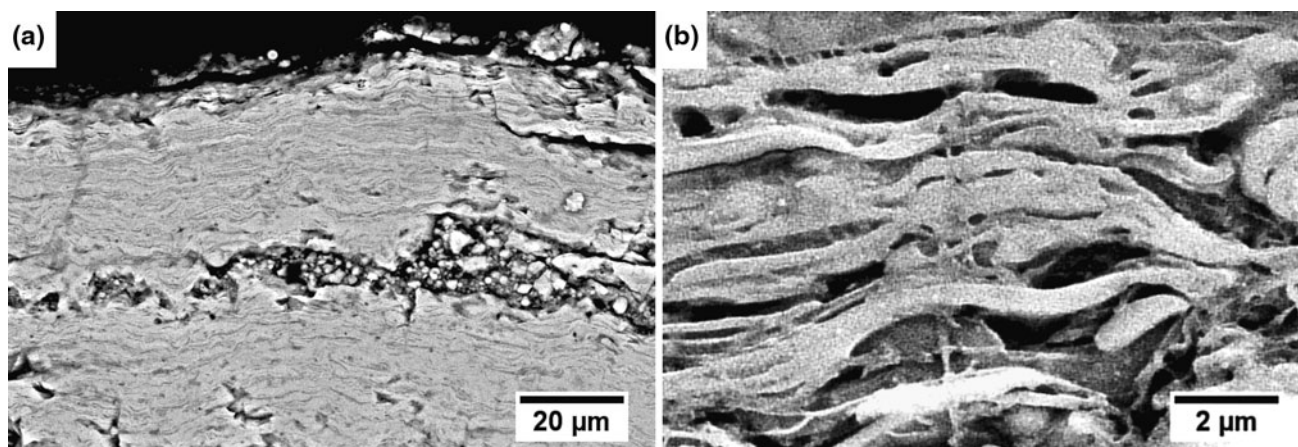


**Fig. 15** Cross-sectional view of the DEG-based HAp coating (advanced CC design) after soaking in SBF for 14 days: second and third layer (a) and detail of the bottom layer showing “etched” lamellae (b)

behaviour of the poorly-crystalline coatings (Fig. 13b). The solution, which managed to penetrate down to the bottom layer through interconnected pores and cracks, probably caused selective dissolution of the most amorphous lamellae: this layer indeed possesses lower crystallinity than the second and third ones (Section 3.3). The bottom layer is therefore not as stable as the rest of the coating, which could produce adhesion problems in the long period.

## 4. Conclusions

The HVSFS technique was employed to deposit HAp coatings onto titanium plates. The use of different dispersion mediums to prepare the HAp suspensions affects the microstructure and mechanical properties of the resulting coatings more than the process parameters. The variation of the CC design also leads to fairly different process behaviour. The optimized combustion of DEG and propane due to the advanced CC design leads to higher maximum surface temperatures during the coating process and hereby to a huge increase of the deposition efficiency. Not only the deposition efficiency could be increased: also the amount of crystalline HAp was drastically improved using the advanced CC design in combination with the DEG-based suspension, probably because the sprayed lamellae are re-crystallised in-situ, while they cool down to the average surface temperature. Only the bottom layer, close to the substrate, consists of major amounts of amorphous calcium phosphate, most likely due to the fast re-solidification (quenching) of the molten droplets on the cold surface of the Ti plates.

All of the HVSFS coatings exhibit similar tensile adhesion strength values, comparable to those of APS and HVOF coatings.

Verification of the biocompatibility of the HVSFS coatings still has to be investigated. SBF tests could be used as the first step to anticipate the stability and bone bonding ability in vivo of the coatings (Ref 55). Coatings containing substantial amounts of amorphous phase tend to dissolve very rapidly in the SBF solution and to be replaced by a precipitation layer consisting of crystalline HAp. This suggests the potential for good biocompatibility but it also indicates excessively poor stability. The most crystalline layers, obtained using the advanced CC design in combination with the DEG-based suspension, by contrast, react very slowly, indicating better stability.

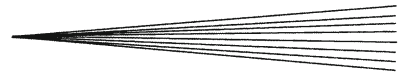
Future developments must aim to produce coatings using a single torch cycle in order to deposit a complete coating with adequate degree of crystallinity. Pre-heating to sufficiently large temperatures and/or the use of bond coats are under investigation in order to achieve this goal. Comparison of the actual in-vitro and in-vivo functionality of HVSFS HAp coatings to that of conventional (plasma- or HVOF-sprayed) coatings will be possible once full optimisation of the former shall have been achieved.

## Acknowledgments

The authors are particularly grateful to Dr. Baldi and Ms. Lorenzi from Cer.i.col for providing the HAp suspension and to Ing. Neda Kollcaku for the precious help with the experimental characterisation activities. This work was partially supported by a grant from the Ministry of Science, Research and Arts of Baden-Württemberg AZ 33-720.830-6-29 to Prof. Dr Gadow.

## References

1. S. Kurtz, E. Lau, M. Halpern, and K. Ong, Trend Shows Growing Orthopedic Surgery Case Load, *Mater. Manag. Health Care*, 2006, **15**(7), p 61-62
2. E. Wintermantel and H. Suk-Woo, *Medizintechnik mit biokompatiblen Werkstoffen und Verfahren*, 3rd ed., Springer, New York, 2002, p 216-228, ISBN 3-540-41261-1 (in German)
3. C.L. Tisdell, V.M. Goldberg, J.A. Parr, J.S. Bensusan, L.S. Staikoff, and S. Stevenson, The Influence of a Hydroxyapatite and Tricalcium-Phosphate Coating on Bone Growth into Titanium Fiber-Metal Implants, *J. Bone Jt. Surg. Am.*, 1994, **76**, p 159-171
4. J. Dumbleton and M.T. Manley, Hydroxyapatite-Coated Prostheses in Total Hip and Knee Arthroplasty, *J. Bone Jt. Surg. Am.*, 2004, **86**, p 2526-2540
5. R. Petit, The Use of Hydroxyapatite in Orthopaedic Surgery: A Ten-Year Review, *Eur. J. Orthop. Surg. Traumatol.*, 1999, **9**, p 71-74
6. L. Sun, C.C. Berndt, K.A. Gross, and A. Kucuk, Materials Fundamentals and Clinical Performance of Plasma-Sprayed Hydroxyapatite Coatings: A Review, *J. Biomed. Mater. Res.*, 2001, **58**, p 570-592
7. K.A. Khor, P. Cheang, and Y. Wang, The Thermal Spray Processing of HA Powders and Coatings, *JOM*, 1997, **49**(2), p 51-57
8. K.A. Khor, H. Li, and P. Cheang, Significance of Melt-Fraction in HVOF Sprayed Hydroxyapatite Particles, Splats and Coatings, *Biomaterials*, 2004, **25**(7), p 1177-1186
9. K. Gross and C. Berndt, Thermal Processing of HA for Coating Production, *J. Biomed. Mater. Res. B*, 1998, **39**(4), p 580-587
10. R.B. Heimann, Recent Trends Towards Improved Plasma-Sprayed Advanced Bioceramic Coatings on Ti6Al4V Implants, *Mat.-wiss. u. Werkstofftech.*, 1999, **30**, p 775-782
11. S. Dyshlovenko, C. Pierlot, L. Pawlowski, R. Tomaszek, and P. Chagnon, Experimental Design of Plasma Spraying and Laser Treatment of Hydroxyapatite Coatings, *Surf. Coat. Technol.*, 2006, **201**, p 2054-2060
12. E. Bouyer, F. Gitzhofer, and M.I. Boulos, Suspension Plasma Spraying for Hydroxyapatite Powder Preparation by R.F. Plasma, *J. Mater. Sci. Lett.*, 1997, **49**(2), p 58-62
13. C. Renghini, E. Girardin, A.S. Fomin, A. Manescu, A. Sabbioni, S.M. Barinov, V.S. Komlev, G. Albertini, and F. Fiori, Plasma Sprayed Hydroxyapatite Coatings from Nanostructured Granules, *Mater. Sci. Eng. B*, 2008, **152**(1-3), p 86-90
14. R.S. Lima, K.A. Khor, H. Li, P. Cheang, and B.R. Marple, HVOF Spraying of Nanostructured Hydroxyapatite for Biomedical Applications, *Mater. Sci. Eng. A*, 2005, **396**, p 181-187
15. H. Li and K.A. Khor, Characteristics of the Nanostructures in Thermal Sprayed Hydroxyapatite Coatings and Their Influence on Coating Properties, *Surf. Coat. Technol.*, 2006, **201**(6), p 2147-2154
16. H. Li, B.S. Ng, K.A. Khor, P. Cheang, and T.W. Clyne, Raman Spectroscopy Determination of Phases Within Thermal Sprayed Hydroxyapatite Splats and Subsequent In Vitro Dissolution Examination, *Acta Mater.*, 2004, **52**, p 445-453
17. K.A. Khor, H. Li, and P. Cheang, Significance of Melt-Fraction in HVOF Sprayed Hydroxyapatite Particles, Splats and Coatings, *Biomaterials*, 2004, **25**, p 1177-1186



18. K.A. Gross, S. Saber-Samandari, and K.S. Heemann. Evaluation of Commercial Implants with Nanoindentation Defines Future Development Needs for Hydroxyapatite Coatings, *J. Biomed. Mater. Res. B*, 2010, **93**(1), p 1-8
19. N. Cao, J. Dong, Q. Wang, Q. Ma, C. Xue, and M. Li, An Experimental Bone Defect Healing with Hydroxyapatite Coating Plasma Sprayed on Carbon/Carbon Composite Implants, *Surf. Coat. Technol.*, 2010, **205**(4), p 1150-1156
20. R.W. Trice and K.T. Faber, Role of Lamellae Morphology on the Microstructural Development and Mechanical Properties of Small-Particle Plasma-Sprayed Alumina, *J. Am. Ceram. Soc.*, 2000, **83**(4), p 889-896
21. C. Monterrubio-Badillo, H. Ageorges, T. Chartier, J.F. Coudert, and P. Fauchais, Preparation of LaMnO<sub>3</sub> Perovskite Thin Films by Suspension Plasma Spraying for SOFC Cathodes, *Surf. Coat. Technol.*, 2006, **200**, p 3743-3756
22. F.-L. Toma, G. Bertrand, D. Klein, C. Coddet, and C. Meunier, Nanostructured Photocatalytic Titania Coatings Formed by Suspension Plasma Spraying, *J. Therm. Spray Technol.*, 2006, **15**(4), p 587-592
23. F.-L. Toma, G. Bertrand, S. Begin, C. Meunier, O. Barres, D. Klein, and C. Coddet, Microstructure and Environmental Functionalities of TiO<sub>2</sub>-Supported Catalysts Obtained by Suspension Plasma Spraying, *Appl. Catal. B*, 2006, **68**, p 74-84
24. A. Killinger, M. Kuhn, and R. Gadow, High-Velocity Suspension Flame Spraying (HVSFS), a New Approach for Spraying Nanoparticles with Hypersonic Speed, *Surf. Coat. Technol.*, 2006, **201**(5), p 1922-1929
25. X.Q. Ma, J. Roth, D.W. Gandy, and G.J. Frederick, A New High-Velocity Oxygen Fuel Process for Making Finely Structured and Highly Bonded Inconel Alloy Layers from Liquid Feedstock, *J. Therm. Spray Technol.*, 2006, **15**, p 670-675
26. R. Rampon, F.-L. Toma, G. Bertrand, and C. Coddet, Liquid Plasma Sprayed Coatings of Yttria-Stabilized Zirconia for SOFC Electrolytes, *J. Therm. Spray Technol.*, 2006, **15**(4), p 682-688
27. P. Fauchais, R. Etchart-Salas, V. Rat, J.F. Coudert, N. Caron, and K. Wittmann-Ténéze, Parameters Controlling Liquid Plasma Spraying: Solutions, Sols, or Suspensions, *J. Therm. Spray Technol.*, 2008, **17**(1), p 31-59
28. R. Gadow, A. Killinger, M. Kuhn, and D. López, Hochgeschwindigkeitssuspensionsflammspritzen, Deutsche Patentanmeldung Nr. DE 10 2005 038 453 A1 (in German)
29. *Thermal Spray 2009: Expanding Thermal Spray Performance to New Markets and Applications*, B.R. Marple, M.M. Hyland, Y.-C. Lau, C.-J. Li, R.S. Lima, and G. Montavon, Eds., 4-7 May 2009(Las Vegas, NV), ASM International, 2009, p 150-155
30. T. Kokubo and H. Takadama, How Useful is SBF in Predicting In Vivo Bone Bioactivity?, *Biomaterials*, 2006, **27**, p 2907-2915
31. A. Killinger, M. Kuhn, and R. Gadow, High-Velocity Suspension Flame Spraying (HVSFS), a New Approach for Spraying Nanoparticles with Hypersonic Speed, *Surf. Coat. Technol.*, 2006, **201**, p 1922-1929
32. R. Lietzow, "Herstellung von Nanosuspensionen mittels Entspannung überkritischer Fluide", Ph.D. Thesis, Universität Karlsruhe, Cuvillier-Verlag, 2006, ISBN 978-3-86727-080-9 (in German)
33. C. Synowietz and K. Schäfer, *Chemiker-Kalender*, 3rd ed., C. Synowietz and K. Schäfer, Eds., 1984, Springer, 1984, ISBN 3-540-12652-x
34. L. Pawlowski, Finely Grained Nanometric and Submicrometric Coatings by Thermal Spraying: A Review, *Surf. Coat. Technol.*, 2008, **202**(18), p 4318-4328
35. R. Gadow, A. Killinger, and N. Stiegler, Hydroxyapatite Coatings for Biomedical Applications Deposited by Different Thermal Spray Techniques, *Surf. Coat. Technol.*, 2010, **205**, p 1157-1164
36. K. VanEvery, M.J.M. Krane, R.W. Trice, H. Wang, W. Porter, M. Besser, D. Sordelet, J. Ilavsky, and J. Almer, Column Formation in Suspension Plasma-Sprayed Coatings and Resultant Thermal Properties, *J. Therm. Spray Technol.*, 2011, **20**, p 817-828
37. G. Bolelli, V. Cannillo, R. Gadow, A. Killinger, L. Lusvardi, J. Rauch, and M. Romagnoli, Effect of the Suspension Composition on the Microstructural Properties of High Velocity Suspension Flame Sprayed (HVSFS) Al<sub>2</sub>O<sub>3</sub> Coatings, *Surf. Coat. Technol.*, 2010, **204**(8), p 1163-1179
38. E. Dongmo, A. Killinger, M. Wenzelburger, and R. Gadow, Numerical Approach and Optimization of the Combustion and Gas Dynamics in High Velocity Suspension Flame Spraying (HVSFS), *Surf. Coat. Technol.*, 2009, **203**(15), p 2139-2145
39. U. Posset, E. Löcklin, R. Thull, and W. Kiefer, Vibrational Spectroscopic Study of Tetracalcium Phosphate in Pure Polycrystalline Form and as a Constituent of Self-Setting Bone Cement, *J. Biomed. Mater. Res.*, 1998, **40**, p 640-645
40. R. Cuscò, F. Guitián, S. de Aza, and L. Artús, Differentiation Between Hydroxyapatite and Beta-Tricalcium Phosphate by Means of Micro-Raman Spectroscopy, *J. Eur. Ceram. Soc.*, 1998, **18**(9), p 1301-1305
41. R.B. Heimann, Thermal Spraying of Biomaterials, *Surf. Coat. Technol.*, 2006, **201**(5), p 2012-2019
42. S. Dyshlovenko, L. Pawlowski, B. Pateyron, I. Smurov, and J.H. Harding, Modelling of Plasma Particle Interactions and Coating Growth for Plasma Spraying of Hydroxyapatite, *Surf. Coat. Technol.*, 2006, **200**, p 3757-3769
43. R. Jaworski, C. Pierlot, L. Pawlowski, M. Bigan, and M. Quivrin, Synthesis and Preliminary Tests of Suspension Plasma Spraying of Fine Hydroxyapatite Powder, *J. Therm. Spray Technol.*, 2008, **17**(5-6), p 679-684
44. P. Fauchais, M. Fukumoto, A. Vardelle, and M. Vardelle, Knowledge Concerning Splat Formation: An Invited Review, *J. Therm. Spray Technol.*, 2004, **13**(3), p 337-360
45. C. Chang, J. Huang, J. Xia, and C. Ding, Study on Crystallization Kinetics of Plasma Sprayed Hydroxyapatite Coating, *Ceram. Int.*, 1999, **25**, p 479-483
46. C.T. Crowe, T.R. Troutt, and J.N. Chung, Numerical Models for Two-Phase Turbulent Flows, *Annu. Rev. Fluid Mech.*, 1996, **28**, p 11-43
47. P.C. Huang, J. Heberlein, and E. Pfender, Particle Behavior in a Two-Fluid Turbulent Plasma Jet, *Surf. Coat. Technol.*, 1995, **73**, p 142-151
48. M. Ivosevic, R.A. Cairncross, and R. Knight, 3D Predictions of Thermally Sprayed Polymer Splats: Modeling Particle Acceleration, Heating and Deformation on Impact with a Flat Substrate, *Int. J. Heat Mass Transf.*, 2006, **49**, p 3285-3297
49. V.R. Srivatsan and A. Dolatabadi, Simulation of Particle-Shock Interaction in a High Velocity Oxygen Fuel Process, *J. Therm. Spray Technol.*, 2006, **15**(4), p 481-487
50. J. Oberste Berghaus, J.-G. Legoux, C. Moreau, F. Tarasi, and T. Chráska, Mechanical and Thermal Transport Properties of Suspension Thermal-Sprayed Alumina-Zirconia Composite Coatings, *J. Therm. Spray Technol.*, 2008, **17**(1), p 91-104
51. S.W.K. Kweh, K.A. Khor, and P. Cheang, Plasma-Sprayed Hydroxyapatite (HA) Coatings with Flame-Spheroidized Feedstock: Microstructure and Mechanical Properties, *Biomaterials*, 2000, **21**(12), p 1223-1234
52. H.C. Gledhill, I.G. Turner, and C. Doyle, In Vitro Dissolution Behaviour of Two Morphologically Different Thermally Sprayed Hydroxyapatite Coatings, *Biomaterials*, 2001, **22**(7), p 695-700
53. S.-W. Ha, R. Reber, K.-L. Eckert, M. Petitmermet, J. Mayer, E. Wintermantel, C. Baerlocher, and H. Gruner, Chemical and Morphological Changes of Vacuum-Plasma-Sprayed Hydroxyapatite Coatings During Immersion in Simulated Physiological Solutions, *J. Am. Ceram. Soc.*, 1998, **81**, p 81-88
54. D. Lahiri, A.P. Benaduce, F. Rouzaud, J. Solomon, A.K. Keshri, L. Kos, and A. Agarwal, Wear Behavior and In Vitro Cytotoxicity of Wear Debris Generated from Hydroxyapatite-Carbon Nanotube Composite Coating, *J. Biomed. Mater. Res. A*, 2011, **96**(1), p 1-12
55. M. Bohner and J. Lemaître, Can Bioactivity be Tested In Vitro with SBF Solution?, *Biomaterials*, 2009, **30**, p 2175-2179